ELECTRONIC STATES OF $Fe_2S^{-/0/+}$

Olaf HÜBNER[1] and Joachim SAUER[2,*]

Humboldt-Universität zu Berlin, Arbeitsgruppe Quantenchemie, Unter den Linden 6, D-10099 Berlin, Germany; e-mail: [1] olaf.huebner@chemie.uni-karlsruhe.de, [2] js@chemie.hu-berlin.de

Received October 1, 2002
Accepted December 14, 2002

Dedicated to Professors Petr Čársky, Ivan Hubač and Miroslav Urban on the occasion of their 60th birthdays.

The relative energies of a multitude of low-lying electronic states of $Fe_2S^{-/0/+}$ are determined by complete active space self-consistent field (CASSCF) calculations. The numerous states obtained are assigned to spin ladders. For selected states, dynamic correlation has been included by multireference configuration interaction (MRCI) and the structures of some high-spin states have been optimized by CASSCF/MRCI. Comparison is made with structures obtained by density-functional theoretical calculations. The ground states of $Fe_2S^{-/0/+}$ are $^{10}B_2$, $^1A_1$ and $^8A_2$, respectively, and the total splittings of the lowest-energy spin ladders are about 0.18, 0.07 and 0.13 eV, respectively. The spin ladders of Fe_2S qualitatively reflect the picture of Heisenberg spin coupling. While both Fe_2S^- and Fe_2S^+ show an Fe–Fe distance of about 270 pm, that of Fe_2S is about 100 pm longer. The calculated adiabatic electron affinity of Fe_2S is 1.2 eV and the ionization energy 6.6 eV. An interpretation of the observed photoelectron spectrum of Fe_2S^- is given.

Keywords: Iron sulfur clusters; Electronic structure; Spin ladders; Multireference configuration interaction; Complete active space SCF; *Ab initio* calculations.

Iron sulfur clusters are the active centres in a variety of proteins[1]. In the gas phase differently charged naked Fe_nS_m [2–9], FeS_n [10–15] and FeS [16–26] species were prepared and their intrinsic properties studied. However, details of the electronic or molecular structures are only known in a few cases. The $FeS^{-/0/+}$ species[15,20,22–27] have been studied by different quantum chemical methods, while for $FeS_2^{-/0/+}$ [15,27], $Fe_2S_2^{-/0/+/2+}$ [27] and related fragments[27] density-functional theoretical (DFT) calculations have been reported. The $Fe_2S_2^{-/0/+/2+}$ species have been examined by complete active space self-consistent field (CASSCF) and multireference configuration interaction (MRCI) calculations[28].

doi:10.1135/cccc20030405

The goal of the present study is to explore the manifold of electronic states of $Fe_2S^{-/0/+}$ and to determine the geometrical structures in the different redox states. Assuming that (i) the electronic structure of neutral Fe_2S can be described as two $Fe^I(d^6s^1)$ and $S^{2-}(s^2p^6)$, (ii) the electrons of a given iron centre are high-spin coupled and (iii) the electrons located at the different centres interact only weakly, a number of low-lying electronic states of different spin is expected. These states belong to the so-called Heisenberg spin ladders[29–31] and show an increasing separation beween levels of increasing spin ($E_i = -JS_i(S_i + 1)$). They arise, among others, from the different possibilities to distribute 14 electrons over the 12 MOs that can be constructed from the 3d and 4s orbitals on the Fe atoms (Fig. 1). As expected from the assumption of $Fe^I(d^6s^1)$ and confirmed by the calculations (*vide infra*), the total occupation of MOs formed from the two 4s orbitals is always two and, therefore, two MOs within the 3d space need to be doubly occupied. Since pairs of 3d orbitals, belonging to different irreducible representations, can be doubly occupied, several different spin ladders are expected. According to the coupling of two Fe^I with local $S = 5/2$, the states of a given spin ladder should vary between singlet (low-spin) and undecet (high-spin). For the systems Fe_2S^- and Fe_2S^+ with an odd number of spins in the 3d and 4s orbitals, the spin ladders are not expected to be of Heisenberg type, at least when assuming delocalized valencies.

This study of $Fe_2S^{+/0/-}$ follows our previous one on $Fe_2S_2^{2+/+/0/-}$ [28]. We first report CASSCF results and discuss the states found in terms of different spin ladders. Subsequently, dynamic correlation is included by MRCI, but this is

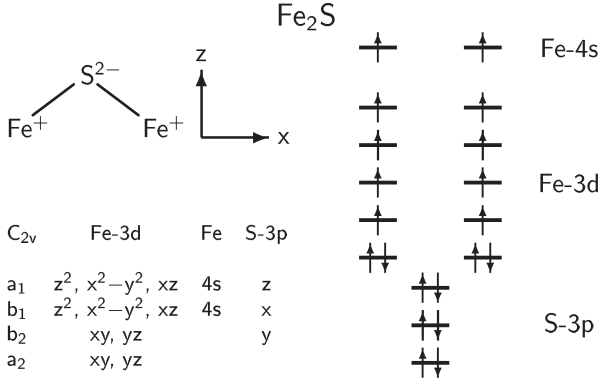

FIG. 1
Orientation of Fe_2S in the Cartesian coordinate system, assignment of the symmetry-adapted combinations of atomic valence orbitals to the irreducible representations of the C_{2v} point group and qualitative scheme of the valence orbitals

only possible for the states of highest spin. Assuming that the dynamic correlation does not change the qualitative pattern of state energies, the MRCI difference of two high-spin states is used to estimate the relative energies of the states of lower spin. This procedure is backed by the studies of Fink *et al.*[32,33] on dimer clusters of transition metals Ti, V, Cr and Ni. These authors have shown that CASSCF calculations are able to provide a qualitative description of the spin coupling whereas quantitative estimates of the spin coupling require the inclusion of dynamic correlation. Further support comes from the work of Mödl *et al.*[34,35] on a thioferrate cluster. MRCI is also used to optimize the structures of $Fe_2S^{+/0/-}$ in high-spin states.

This study, like that on of Fe_2S_2 [28], neither includes scalar relativistic contributions nor spin orbit couplings. Scalar relativistic effects are expected to be very small[24]. Spin-orbit coupling could affect the splitting by less than 0.1 eV, the total spin-orbit splitting for the free atom[36], but would be most important for a symmetrical (*e.g.* octahedral) environment of the iron centres and less important in the present case.

COMPUTATIONAL DETAILS

The calculations use the MOLPRO 96 program with the internal contraction scheme for the MRCI calculations[37–42]. Cluster corrections are evaluated using both the Davidson and Pople formulas. We generally refer to the Davidson correction, denoted +Q, while results of the Pople correction will only be mentioned when they are significantly different. For comparison, some splittings are calculated using the averaged quadratic coupled cluster (AQCC) functional[43]. The basis sets for Fe/S are [6s4p3d2f/5s4p3d]; atomic natural orbital contractions are taken from Pierloot *et al.*[44]

The calculations are performed in C_{2v} symmetry. A first series of calculations of the spin ladders of Fe_2S, Fe_2S^- and Fe_2S^+ uses structures obtained by DFT calculations[27] with the B3LYP exchange-correlation functional[45,46] and the TZVDP/TZVEP [6s5p3d/6s4p1d] basis sets[47] on Fe/S from Ahlrichs' group, which include the two p functions of Wachters on iron[48]. The TURBOMOLE program[49,50] is employed. Subsequently, the structures for the high-spin states of the lowest energy spin ladders of Fe_2S and Fe_2S^- are optimized by MRCI and the calculation of the spin ladders repeated at those structures (Table VI). For Fe_2S^+, the calculations of the spin ladders are not repeated, as the (symmetrized) B3LYP structure used (d(Fe–Fe) = 261.3 and d(Fe–S) = 217.7 pm, the mean value of 216.7 and 218.7 pm for the B3LYP $^8A''$ structure[27]) has proven to be close to the MRCI+Q optimized structure of the $^8A_1$ term (Table VI).

For selected high-spin states only, the structures are optimized by CASSCF/MRCI calculations. Assuming C_{2v} symmetry, the CASSCF/MRCI energy is calculated for a two-dimensional grid of different Fe–Fe and Fe–S distances, followed by a polynomial fit of the potential energy surface. Then the minimum of the fit function is determined analytically. A second set of DFT structure optimizations is made for comparison with MRCI structure predictions.

RESULTS

CASSCF Calculations

This section provides an overview over the numerous electronic states that result from different 3d occupations and different spin-coupling, and assigns them to spin ladders. Tables I and II show the occupation of the natural orbitals for the high-spin terms of the different spin ladders for $Fe_2S^{0/-}$ and Fe_2S^+, respectively. The occupations for the other multiplicities of a given ladder are similar. The states of one spin ladder alternate between two different irreducible representations of A and B type. In the following a spin ladder will be named after the irreducible representation of its low-spin term, *i.e.* the singlet term for Fe_2S and the doublet term for Fe_2S^- and Fe_2S^+.

The ten Fe 3d, two Fe 4s and three S 3p orbitals generate the full valence orbital space of Fe_2S. Figure 1 shows the irreducible representations of the

TABLE I
Occupation[a] of the natural orbitals from CASSCF calculations for the high-spin states of the different spin ladders of Fe_2S and Fe_2S^-

Fe_2S and Fe_2S^- Fe-3d					State	Fe_2S Spin ladder	Fe-4s		State	FeS^- Spin ladder	Fe-4s	
b_1	b_1	b_1	a_2	a_2								
a_1	a_1	a_1	b_2	b_2			a_1	b_1			a_1	b_1
2	1	1	1	1	$^{11}B_1$	A_1	1	1	$^{8}B_1$,$^{10}B_1$	A_1,B_1	2	1
1.5	1.5	1	1	1	$^{11}A_1$	B_1	1	1				
1.5	1	1	1.5	1	$^{11}A_2$,$^{11}B_2$	B_2, A_2	1	1	$^{10}B_2$,$^{10}A_2$	B_2,A_2	2	1

[a] Occupations denoted by 1.5 vary between 1.4 and 1.6, occupations denoted by 1 vary between 0.9 and 1.1

C_{2v} point group to which the symmetry-adapted combinations of atomic orbitals belong. For Fe_2S and Fe_2S^-, the active space for the CASSCF calculations is defined by the twelve Fe 3d and 4s orbitals. However, for the spin ladders with a pair of doubly occupied Fe 3d orbitals (A_1 of Fe_2S, and A_1 and B_1 of Fe_2S^-, see Table I), the active space is reduced to ten orbitals by closing the two doubly occupied Fe 3d orbitals.

For Fe_2S^+ these valence spaces are extended by the three S 3p orbitals. An active space with 13 orbitals is obtained for spin ladders with a pair of doubly occupied Fe 3d orbitals, while a space of 15 orbitals is obtained for the remaining spin ladders. However, this 15-orbital space is applied to the two states of highest spin of a given spin ladder only, while for the complete set of all states of these spin ladders an active space of 11 orbitals is used, which consists of the ten Fe 3d orbitals and the bonding combination (a_1) of the Fe 4s orbitals. In the latter case, the energy levels of the doublet and quartet terms are obtained by scaling the energy splittings, calculated with eleven active orbitals, with the ratio of the sextet–octet splitting obtained with fifteen and eleven orbitals.

Figure 2 shows the terms of the different spin ladders of $Fe_2S^{-/0/+}$. The size of the spin coupling and the spread of the spin ladders depends on the Fe–Fe distance. In Fe_2S this distance is very long (371 pm), while it is significantly shorter in $Fe_2S^{+/-}$. Hence the high-spin/low-spin splitting is much larger in $Fe_2S^{+/-}$, while in neutral Fe_2S, all states of a given spin ladder are close together.

TABLE II
Occupation[a] of the natural orbitals from CASSCF calculations for the high-spin states of the different spin ladders of Fe_2S^+

State	Spin ladder	Fe-4s3d		Fe-3d				
				b_1	b_1	b_1	a_2	a_2
		a_1	a_1	a_1	a_1	–	b_2	b_2
$^{10}A_1$	A_1	1	1	2	1	1	1	1
$^8A_1$	B_1	1.6	0.4	2	1	1	1	1
$^8A_2$, $^8B_2$	B_2,A_2	1.6	0.4	1.5	1	1	1.5	1

[a] Occupations denoted by 1.5 vary between 1.4 and 1.6

Fe_2S. The heights of the different spin ladders are smaller than 0.03 eV. Figure 3 is an enlarged representation of the states shown in Fig. 2, middle. All the spin ladders show an antiferromagnetic coupling, with the lowest term being a singlet. They approximately reflect the pattern of Heisenberg spin coupling. For all spin ladders, the electrons in the 3d orbitals as well as those in the 4s orbitals contribute to the antiparallel spin coupling and, therefore, spin ladders with six levels between singlet and undecet are observed. Obviously, the different nature of 3d and 4s orbitals does not induce a different coupling, at least not in the presence of the large distance between the iron centres. Figure 4 shows the energy and character of the natural orbitals for the $^9A_1$ term. The composition of the orbitals for the other states of Fe_2S is virtually the same. The natural orbitals for the states of all spin ladders include three doubly occupied orbitals that are essentially sulfur 3p orbitals, ten orbitals with an occupation of 12 electrons that are essentially iron 3d orbitals, and two singly occupied, predominantly iron 4s orbitals. Hence, the assumption is confirmed that Fe_2S can be considered as $Fe^{I}{}_2S^{-II}$, but the observed orbital admixtures indicate covalent contributions to the Fe–S interaction, mainly from the mixing of two S 3p orbitals (b_1, a_1) with the Fe 4s orbitals. The single occupation of both the bonding and antibonding combinations of 4s orbitals yields formally no iron–iron bonding.

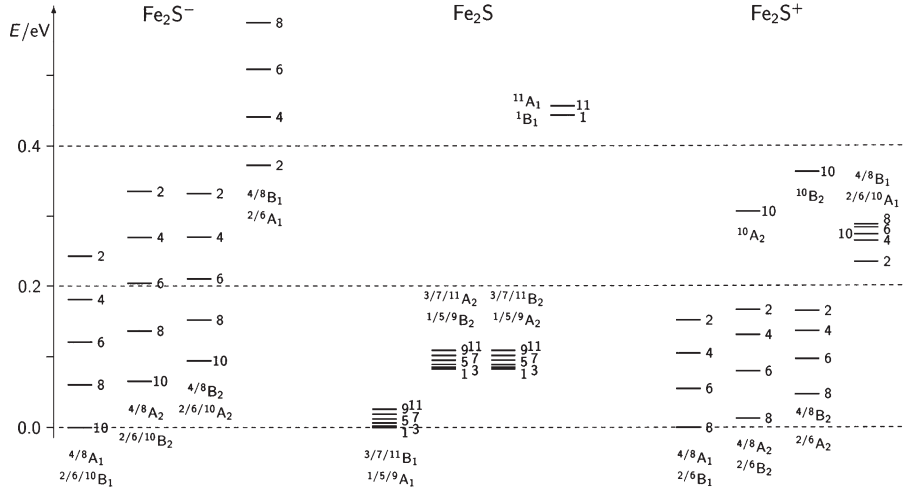

FIG. 2
Spin ladders for Fe_2S^-, Fe_2S and Fe_2S^+ by CASSCF calculations

The ground state of Fe_2S is $^1A_1$. The B_2 and A_2 spin ladders lie only 0.08 eV higher, the B_1 spin ladder 0.4 eV. The ground-state A_1 spin ladder (high-spin term $^{11}B_1$) shows two doubly occupied 3d orbitals. This permits the use of an active space of ten orbitals generated by closing the two doubly occupied 3d orbitals (a_1, b_1) for the states of the A_1 spin ladder. In contrast, the B_1, B_2 and A_2 spin ladders (with high-spin terms $^{11}A_1$, $^{11}A_2$ and $^{11}B_2$, respectively) are characterized by four 3d orbitals with an average occupation of 1.5 electrons. Their states emerge from the mixing of two configurations with different doubly occupied 3d orbitals. Hence, for calculations of states belonging to the B_1, B_2 and A_2 spin ladders, the full active space of the twelve orbitals with all the Fe 3d and 4s orbitals is used.

Fe_2S^-. All the spin ladders (Fig. 2) are characterized by nearly equidistant levels similarly to the spin ladders of $Fe_2S_2^-$ [28]. The A_1 spin ladder shows an antiferromagnetic coupling, while the three other spin ladders show a ferromagnetic coupling with the decet as the lowest term. The lowest term of Fe_2S^- is $^{10}B_1$; the B_2 and A_2 spin ladders lie only 0.07 and 0.09 eV higher, respectively, the A_1 spin ladder about 0.4 eV higher. The heights of the different spin ladders vary beween 0.2 and 0.3 eV.

The natural orbital occupation (Table I) differs from that of neutral Fe_2S by an additional electron in the bonding combination of the predominantly 4s orbitals. This implies a formal Fe–Fe bond order 1/2 and also makes Fe_2S^- a delocalized $Fe^0Fe^{I}S^{-II}$ system. The energy pattern of the natural orbitals for the $^{10}B_1$ term is qualitatively the same as that for the $^9A_1$

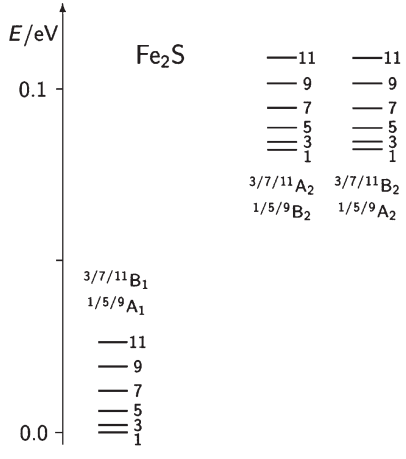

FIG. 3
Spin ladders for Fe_2S by CASSCF calculations, enlarged part of Fig. 2

term of Fe_2S (Fig. 4), except a shift to higher energies. The composition of the orbitals for the other states of Fe_2S^- is similar to that shown for the $^{10}B_1$ term. The spin ladders differ not only by the occupation of the 3d shell, but also by the way of coupling between the 4s electron in the b_1 orbital and the 3d electrons. For the B_2 and A_2 spin ladders, the unpaired 4s electron shows a parallel coupling with the 3d shell. The A_1 and B_1 spin ladders ($^8B_1$ and $^{10}B_1$ high-spin terms) have the same 3d occupation as the A_1 spin ladder of Fe_2S, but they differ in the coupling of the 4s-b_1 electron with the 3d shell, which is parallel in the B_1 case and antiparallel in the A_1 case.

Comparison of the present results for Fe_2S and Fe_2S^- with those for Fe_2S_2 and $Fe_2S_2^-$ [28] shows that the spin ladders of both anions have nearly equidistant levels, while both neutral systems are characterized by Heisenberg spin ladders with increasing energy gaps. Hence, the spin coupling in both Fe_2S^- and $Fe_2S_2^-$ is dominated by the unpaired 4s electron.

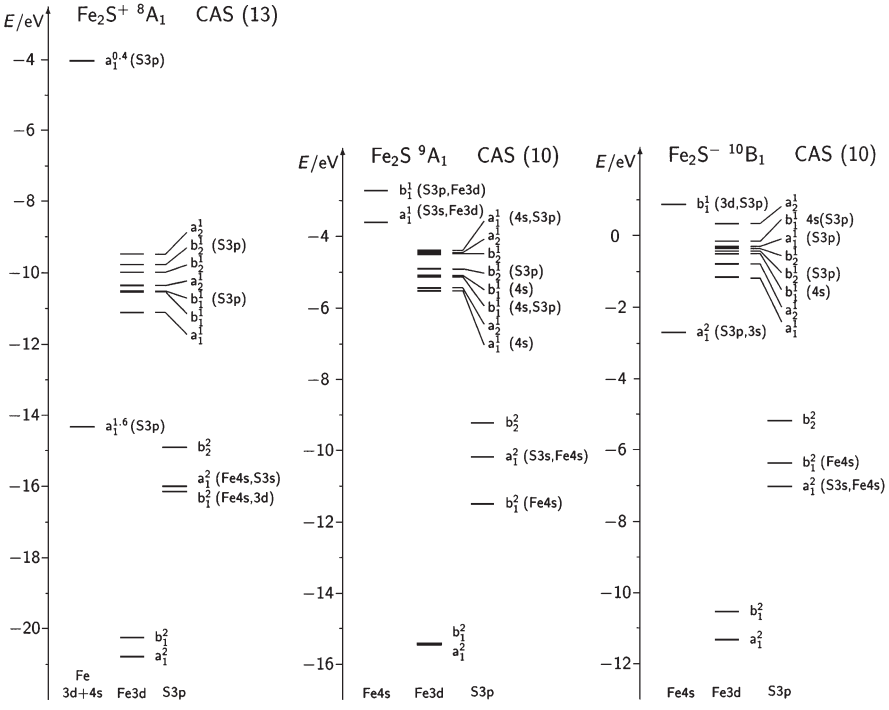

FIG. 4
Orbital energies for the $^8A_1$, $^9A_1$ and $^{10}B_1$ states of Fe_2S^+, Fe_2S and Fe_2S^-, respectively, by CASSCF calculations

Fe_2S^+. The heights of the different spin ladders vary between about 0.05 and 0.15 eV (Fig. 2). The three lowest spin ladders (B_1, B_2 and A_2) show a ferromagnetic coupling with the octets $^8A_1$, $^8A_2$ and $^8B_2$, respectively, as the lowest terms. The lowermost among them is $^8A_1$; although, the $^8A_2$ and $^8B_2$ terms are only 0.01 and 0.05 eV higher. The A_1 spin ladder is found at 0.2 eV. Furthermore, $^{10}A_2$ and $^{10}B_2$ terms are found at a relative energy of 0.3 eV above the $^8A_2$ and $^8B_2$ terms, respectively.

For the states of all spin ladders, besides three doubly occupied, essentially sulfur 3p orbitals, there are nine essentially iron 3d orbitals occupied with eleven electrons and two sd hybrid orbitals occupied by two electrons (Table II). Hence, Fe_2S^+ can be considered as delocalized $Fe^{I}Fe^{II}S^{-II}$. The occupation of the bonding a_1 combination of the 4s orbitals indicates the formal Fe–Fe bond order 1/2. Figure 4 shows the energy and character of the natural orbitals for the $^8A_1$ term. The composition of the natural orbitals for the other states of Fe_2S^+ is almost the same. The A_1 and B_1 spin ladders have the same 3d occupation but differ in the coupling of the electrons of the sd hybrid orbitals. For the $^{10}A_1$ term of the A_1 spin ladder, all spins are necessarily parallelly aligned. For the states of lower spin, the electrons of the 3d as well as of the sd hybrid orbitals contribute to the antiparallel coupling in a similar manner. For higher spin states, the different nature of the 3d and 4s electrons probably leads to the complex splitting pattern. In contrast, for the B_1 spin ladder, the electrons of the sd hybrid orbitals show an antiparallel coupling, and the leading configurations are characterized by double occupation of the lower-lying sd hybrid orbital. Hence, the state of highest multiplicity of this coupling is an octet. For the B_2 and A_2 spin ladders, the coupling of the electrons of the sd hybrid orbitals is analogous to that of the B_1 spin ladder. The $^{10}A_2$ and $^{10}B_2$ terms (Fig. 2) have the same 3d configurations as the $^8A_2$ and $^8B_2$ octets, respectively, but necessarily a parallel coupling of the electrons in the sd hybrid orbitals. Because of the uneven number of unpaired 3d electrons, the spin coupling is not of Heisenberg type.

MRCI Calculations

Only the electrons in the Fe 3d and 4s and S 3p orbitals are included in the MRCI correlation treatment. For Fe_2S the reference spaces include all configurations having a coefficient larger than 0.01 in the respective CASSCF wavefunctions. For Fe_2S^- the reference spaces are identical to the active spaces of the CASSCF calculations. MRCI calculations for Fe_2S^+ use the orbitals from the CASSCF calculations with thirteen or fifteen orbitals,

while the reference spaces are built by closing the three essentially doubly occupied sulfur orbitals and by excluding the weakly occupied antibonding combination of the Fe 4s orbitals.

Fe_2S. Table III shows various relative energies at the MRCI+Q structure of Fe_2S ($^9A_1$). Inclusion of dynamic correlation by MRCI increases the CASSCF result for the $^{11}B_1$–$^9A_1$ splitting from 7 to 15 meV. Cluster corrections increase this value to 20 and 78 meV when applying the Davidson and Pople formulas, respectively. Similarly, MRCI increases the CASSCF value of the $^9A_1$–$^7B_1$ splitting from 7 to 14, 18 and 60 meV (MRCI, MRCI+Q and MRCI+Q^{Pople}, respectively). In both cases the Pople formula predicts a considerably larger correction. AQCC calculations yield 19 and 16 meV for the two splittings, which supports the Davidson corrected results. Therefore, reference will be made hereinafter to Davidson corrected values only. For the $^9A_1$–$^1A_1$ splitting, an estimate of 49 meV is obtained, assuming that MRCI+Q has the same effect on the $^9A_1$–$^1A_1$ splitting as it has on the $^9A_1$–$^7B_1$ splitting (Table III). For the total $^{11}B_1$–$^1A_1$ splitting of the A_1 spin ladder, an estimate of 69 meV is obtained from the $^9A_1$–$^1A_1$ splitting

TABLE III
Relative energies (meV) of various states of Fe_2S obtained by MRCI in two different structures

Structure	State	CASSCF	MRCI	+Q	AQCC
$Fe_2S(^9A_1)$	$^{11}B_1$–$^9A_1$	7	15	20	19
	$^9A_1$–$^7B_1$	7	14	18	16
	$^9A_1$–$^1A_1$	19		(49)[a]	
	$^{11}A_2$–$^9B_2$	7	16	21	
	$^9B_2$–$^9A_1$	82	55	43	
	$^{11}B_2$–$^9A_2$	7	16	21	
	$^9A_2$–$^9A_1$	82	55	42	
	$^{11}A_1$–$^{11}B_1$	429	371	342	
$Fe_2S^-(^{10}B_2)$	$^{11}B_1$–$^9A_1$	73	123	148	
	$^9A_1$–$^7B_1$	64	87	103	
	$^9A_1$–$^1A_1$	156		(251)[a]	
	$^{11}B_2$–$^9A_2$	81	129	157	
	$^9A_2$–$^9A_1$	72	31	6	

[a] Estimated, see the main text.

(49 meV) and the MRCI+Q result for the $^{11}B_1$–$^9A_1$ splitting (20 meV). For the high-spin states of the B_2 and A_2 spin ladders ($^{11}A_2$–$^9B_2$ and $^{11}B_2$–$^9A_2$), MRCI+Q yields splittings of 21 meV, which is close to the $^{11}B_1$–$^9A_1$ result.

Inclusion of dynamic correlation yields smaller values for the relative energies of the different spin ladders. The $^9B_2$, $^9A_2$, $^{11}A_2$ and $^{11}B_2$ terms are shifted to lower energies by about 40 meV with respect to the states of the A_1 spin ladder having the same multiplicity. The $^{11}A_1$ term lies 342 meV above the $^{11}B_1$ term. However, the relative positions of the spin ladders do not change qualitatively and the $^1A_1$ term remains the ground state.

To assist the interpretation of the PES of Fe_2S^-, MRCI results are also reported for Fe_2S with adopted Fe_2S^- structure. For this structure, the Fe–Fe distance is much smaller and, hence, the splitting of the spin ladders is much larger. Inclusion of dynamic correlation gives $^{11}B_1$–$^9A_1$ and $^9A_1$–$^7B_1$ splittings of 148 and 103 meV, respectively. The MRCI+Q estimate of the $^9A_1$–$^1A_1$ splitting is 251 meV (Table III), which leads to a total splitting between undecet and singlet ($^{11}B_1$–$^1A_1$) of 399 meV . The $^{11}B_2$ and $^9A_2$ terms are only 16 and 6 meV, respectively, above the terms of the same multiplicity belonging to the A_1 spin ladder. This means that the splitting of the two spin ladders is about the same.

Fe_2S^-. Table IV shows relative energies of different states of Fe_2S^- at the minimum structure of the $^{10}B_2$ term. Inclusion of dynamic correlation reduces the $^8A_1$–$^{10}B_1$ splitting from 61 meV (CASSCF) to 54 meV (MRCI) and 45 meV (MRCI+Q). Again, the AQCC result of 46 meV supports the Davidson corrected value. For the total splitting of the B_1 spin ladder, an estimate of 179 meV, including the dynamic correlation, is obtained. Similar values are expected for the total splittings of the B_2 and A_2 spin ladders.

TABLE IV
Relative energies (meV) of various states of Fe_2S^- obtained by MRCI in the structure of the $^{10}B_2$ term

State	CASSCF	MRCI	+Q	AQCC
$^8A_1$–$^{10}B_1$	61	54	45	46
$^2B_1$–$^{10}B_1$	243		(179)[a]	
$^{10}B_2$–$^{10}B_1$	66	–12	–42	
$^{10}A_2$–$^{10}B_1$	94	42	22	

[a] Estimated, see the main text.

In contrast to Fe_2S, dynamic correlation changes the relative positions of the Fe_2S^- spin ladders. MRCI+Q lowers the relative energies of the $^{10}B_2$ and $^{10}A_2$ terms with respect to $^{10}B_1$ by 108 and 72 meV, respectively, compared with the CASSCF results. The $^{10}B_2$ and $^{10}A_2$ terms are now at relative energies of –42 and 22 meV, respectively, and the former one is probably the ground state of Fe_2S^-.

Fe_2S^+. Table V shows different relative energies at the symmetrized B3LYP structure of the $^8A''$ state. MRCI+Q calculations slightly reduce the CASSCF result for the $^6B_1$–$^8A_1$ splitting from 55 to 48 meV. This yields an estimate of 133 meV for the total splitting of the B_1 spin ladder.

MRCI changes the relative energies of the low-lying states of the low-energy spin ladders. The $^8A_2$ and $^8B_2$ terms are 91 and 30 meV, respectively, below the $^8A_1$ term, the lowest term of the CASSCF calculations. Therefore, the likely ground state is $^8A_2$. Since for the total splittings of the B_2 and A_2 spin ladders the same changes can be expected as for the A_1 spin ladder, probably all the states of the lowest spin ladder lie within about 150 meV. The states of higher energy, $^{10}A_1$ and $^8B_1$ of the A_1 spin ladder and the $^{10}B_2$ and $^{10}A_2$ states, are shifted to even higher energies by MRCI.

Structure optimization. Table VI shows the optimized structures for selected high-spin states of Fe_2S, Fe_2S^- and Fe_2S^+. Inclusion of cluster corrections generally slightly shortens bond lengths: Fe–S by about 1 pm and Fe–Fe by 3 to 8 pm.

TABLE V
Relative energies (meV) of various states of Fe_2S^+ obtained by MRCI in the symmetrized B3LYP structure of the $^8A''$ term

State	CASSCF	MRCI	+Q
$^6B_1$–$^8A_1$	55	57	48
$^2B_1$–$^8A_1$	152		(133)[a]
$^8A_2$–$^8A_1$	13	–46	–91
$^8B_2$–$^8A_1$	47	5	–30
$^{10}A_1$–$^8A_1$	274	507	639
$^8B_1$–$^8A_1$	288	481	588
$^{10}A_2$–$^8A_2$	293	560	706
$^{10}B_2$–$^8B_2$	315	589	745

[a] Estimated, see the main text.

In order to ensure convergence to the same states as obtained by the CASSCF calculations, the B3LYP optimizations use C_{2v} symmetry. (Note that the B3LYP calculations[27] yield broken-symmetry structures (C_s) for the high-spin states of $Fe_2S^{+/-}$.) The B3LYP-optimized structures are in good agreement with the MRCI structures, except for the very long Fe–Fe distance for the $^{11}B_1$ term of Fe_2S, which deviates by 30 pm from the MRCI+Q result.

DISCUSSION

Structure and Bonding

While Fe_2S^+ and Fe_2S^- have Fe–Fe distances between 270 and 280 pm, the Fe–Fe distance in neutral Fe_2S is much longer, *viz.* 370 pm (Table VI). These structural changes are in line with a formal Fe–Fe bond order 1/2 for the charged species and zero in neutral Fe_2S (Scheme 1).

A consequence of the long Fe–Fe distance in Fe_2S is a weak coupling between the spins of the two Fe sites. This results in a total splitting of the (lowest-lying) Fe_2S spin ladder of 0.07 eV only, which is noticeably smaller than the splitting of 0.17 eV found previously for Fe_2S_2[28]. In Fe_2S_2 the

TABLE VI
Structures (pm) optimized by CASSCF/MRCI calculations and comparison with B3LYP structures

Species	State	Distance	MRCI	+Q	B3LYP
Fe_2S^-	$^{10}B_1$	Fe–Fe	285.1	279.4	267.3
		Fe–S	233.1	232.3	229.6
	$^{10}B_2$	Fe–Fe	276.2	268.1[a]	
		Fe–S	233.0	232.0[a]	
Fe_2S	$^{11}B_1$	Fe–Fe	379.7	371.9	344.5
		Fe–S	228.5	227.7	227.9
	$^{9}A_1$	Fe–Fe	375.5	370.6[a]	
		Fe–S	228.4	227.9[a]	
Fe_2S^+	$^{8}A_1$	Fe–Fe	268.8	265.8	268.9
		Fe–S	221.0	219.9	217.7

[a] Structures used for CASSCF calculations.

Fe–Fe distance is by about 100 pm shorter. In contrast, the Fe–Fe distances in the anions Fe_2S^- and $Fe_2S_2^-$ only differ by 11 pm and the total splittings of the spin ladders are similar, about 0.18 eV both. Bridging the two Fe sites by one or two S atoms in $Fe_2S^{0/-}$ and $Fe_2S_2^{0/-}$ affects the structure only if there is no Fe–Fe 4s bonding contribution (neutral Fe_2S and Fe_2S_2 systems), but has virtually no influence if there is Fe–Fe 4s bonding.

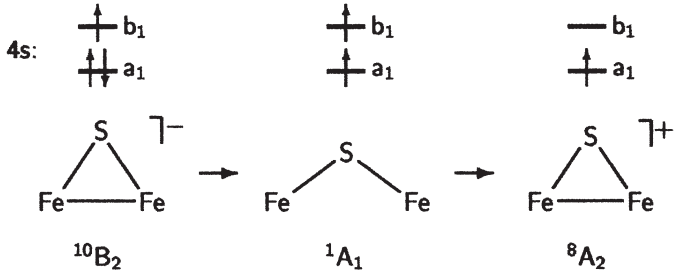

SCHEME 1

The structures of the two considered states of different spin multiplicity of Fe_2S are very similar (both belong to the A_1 spin ladder), the Fe–Fe and Fe–S distances only differing by 1.3 and 0.2 pm, respectively (Table VI). The same is true for the structures of both considered states of Fe_2S^- with a different 3d occupation. The Fe–S distances are virtually identical and the Fe–Fe distances only differ by 11 pm. We conclude that the spin coupling has no great influence on the structures; similarly, different 3d occupations also do not induce large structural changes.

The present multireference *ab initio* computational results for Fe_2S contrast with our former DFT results[27]. Indeed, the $^{11}B_1$ term with a long Fe–Fe distance has also been found by the DFT calculations showing a 30 pm shorter Fe–Fe distance. However, while CASSCF/MRCI predicts the corresponding $^1A_1$ low-spin term only 0.07 eV below the $^{11}B_1$ term, the DFT calculations[27] result in a broken-symmetry low-spin state with a much shorter Fe–Fe distance of 249 pm, as much as 1.13 eV below $^{11}B_1$. In the $^{11}B_1$ high-spin state, the electron configuration is $Fe^I(d^6s^1)_2S^{-II}$. The parallel spin orientation excludes mixing of the 4s with the 3d orbitals, and two 4s electrons with parallel spins occupy the bonding and antibonding combinations of the 4s orbitals. This results in a zero Fe–Fe bond order and a long Fe–Fe distance. In the low-spin state, s-d mixing is possible and the two electrons in the sd orbitals form a weakly bonding pair. The large stabilization of the low-spin state resulting from the B3LYP calculations is driven by the inherent preference of current functionals for larger 3d occupan-

cies[51,52]. Furthermore, the broken-symmetry DFT calculation for the low-spin state does not correctly describe the weak interaction between the two iron centres, as seen by the short Fe–Fe distance. The predominantly iron 4s orbitals of the DFT low-spin state, although essentially localized, show significant contributions from the 4s orbitals of the other iron centre, hence indicating covalent bonding interactions, obviously absent in the CASSCF/MRCI wavefunction.

Electron Affinities and Ionization Energies

Ionization energies are defined as differences between the ground states of the different redox states. As dynamic correlation effects can only be easily calculated for the high-spin states, a problem arises for neutral Fe_2S which has a low-spin ground state. In this case we first calculate the MRCI+Q energy differences, using the high-spin state of Fe_2S, and determine the high-spin/low-spin difference by making use of the estimated spin ladder splitting. In the case of Fe_2S, different structures are used to estimate the difference between the adiabatic electron affinity (AEA) and the vertical electron detachment energy (VDE) of the anion, *i.e.* the nuclear relaxation energy.

For Fe_2S^- a $^{10}B_2$ ground state is assigned. The vertical detachment energy into the $^9A_2$ state of Fe_2S, the lowest-energy final state with a high expected transition probability is 1.57 eV (MRCI+Q). Since the experimental VDE is probably due to the $^7B_2 \leftarrow {}^8A_2$ transition (*vide infra*), we need estimates for the $^8A_2$–$^{10}B_2$ (Fe_2S^-) and $^9A_2$–$^7B_2$ (Fe_2S) splittings. MRCI results are not available, but the splittings are very similar for different low-energy spin ladders. Using the MRCI+Q splittings for $^8A_1$–$^{10}B_1$ (0.05 eV, Table IV) and $^9A_1$–$^7B_1$ (0.10 eV, Table III) and the $^9A_2 \leftarrow {}^{10}B_2$ result (1.57 eV), we get an estimate of 1.42 eV for the VDE. The adiabatic electron affinity is due to the $^1A_1 \leftarrow {}^{10}B_2$ transition. The MRCI+Q energy difference for the high-spin states ($^9A_1 \leftarrow {}^{10}B_2$) of the same spin ladders is 1.23 eV. With the estimate of 49 meV for the $^9A_1$–$^1A_1$ splitting (Table III), the AEA of 1.18 eV is obtained.

These results, 1.42 and 1.18 eV for VDE and AEA, respectively, are lower by merely 0.21 and 0.25 eV, respectively, than the experimental VDE of 1.63 eV and threshold energy of 1.43 eV [6]. This good agreement may be fortuitous, as the corresponding deviations for Fe_2S_2 [28] are significantly larger, about 1 eV.

The MRCI+Q energy difference between the $^8A_1$ term of Fe_2S^+ and the $^9A_1$ term of Fe_2S at the respective MRCI+Q minima is 6.65 eV. Since the ground

states $^8A_2$ (Fe_2S^+) and $^1A_1$ (Fe_2S) lie about 0.09 eV (Table V) and 0.05 eV (Table III), respectively, below these states, our estimate for the ionization energy of Fe_2S is 6.61 eV.

Photoelectron Spectrum of Fe_2S^-

The photoelectron spectrum of Fe_2S^- [6] features one low-lying band (width 0.6 eV) with three maxima at 0.2, 0.3 and 0.45 eV with respect to the onset of the band (Fig. 5). The results of the present study permit an interpretation in terms of transitions from the states of the lowest-energy spin ladder of Fe_2S^- (B_2 spin ladder) into the states of the A_2 spin ladder of Fe_2S. Transitions between the corresponding states of these spin ladders change only the occupation of the 4s a_1 orbital from double to single and, hence, should be most intense. The ground term of the B_2 spin ladder is $^{10}B_2$. The $^8A_2$ term is only 0.04 eV higher. Boltzmann statistics indicates an occupation of 20% (298 K) and, therefore, transitions from this state should be observed. For the vertical transitions from $^8A_2$ to $^7B_2$ and $^9A_2$, and from $^{10}B_2$ to $^9A_2$ and $^{11}B_2$, our calculations yield relative energies of 0, 0.10, 0.14 and 0.30 eV, respectively. These values approximately agree with the observed positions of the maxima (Fig. 5). Of course, unresolved vibrational structures have to be assumed for all transitions. Furthermore, the observed onset of the band (0.45 eV below the maximum assigned to the transition to $^{11}B_1$) agrees with the calculated relaxation energies (0.43 and 0.29 eV for $^{11}B_2$ and $^9A_2$, respec-

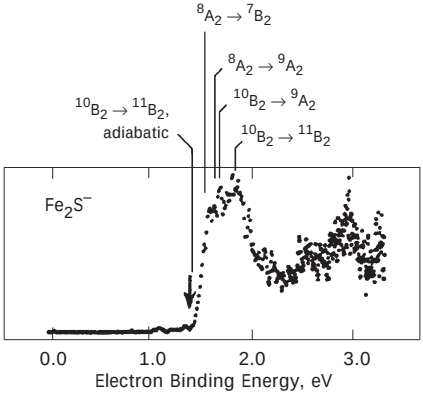

FIG. 5
Experimental photoelectron spectrum of Fe_2S^- and tentative assignments

tively). Transitions from the other low-lying spin ladders of the anion, according to their occupation, may also contribute to the spectrum.

CONCLUSIONS

In all redox states studied, Fe_2S shows low-lying states of different spin that can be assigned to several spin ladders. Compared with the anion and cation, the Fe–Fe distance in neutral Fe_2S is significantly longer. This is explained by the formal Fe–Fe bond order which is zero for neutral Fe_2S and 1/2 for the charged species. The total splitting of the spin ladders of $Fe_2S^{-/0/+}$ reflects the structural changes: it is distinctly smaller for neutral Fe_2S. Neither the different spin couplings within a given spin ladder nor the different 3d occupations of different spin ladders have a large influence on the structures.

This work has been supported by the Deutsche Forschungsgemeinschaft and by the Fonds der Chemischen Industrie. The Konrad Zuse Zentrum für Informationstechnik in Berlin is acknowledged for providing computing time.

REFERENCES

1. Cammack R. in: *Advances in Inorganic Chemistry*, Vol. 38, p. 281. Academic Press, New York 1992.
2. El Nakat J. H., Fisher K. J., Dance I. G., Willett G. D.: *Inorg. Chem.* **1993**, *32*, 1931.
3. Yu Z., Zhang N., Wu X., Gao Z., Zhu Q., Kong F.: *J. Chem. Phys.* **1993**, *99*, 1765.
4. Bililign S., Feigerle C. S., Miller J. C.: *Appl. Surf. Sci.* **1998**, *127–129*, 344.
5. Whetten R. L., Cox D. M., Trevor D. J., Kaldor A.: *J. Phys. Chem.* **1985**, *89*, 566.
6. Zhang N., Hayase T., Kawamata H., Nakao K., Nakajima A., Kaya K.: *J. Chem. Phys.* **1996**, *104*, 3413.
7. Nakajima A., Hayase T., Hayakawa F., Kaya K.: *Chem. Phys. Lett.* **1997**, *280*, 381.
8. Harvey J. N., Schröder D., Schwarz H.: *Inorg. Chim. Acta* **1998**, *273*, 111.
9. Koszinowski K., Schröder D., Schwarz H., Liyanage R., Armentrout P. B.: *J. Chem. Phys.* **2002**, *117*, 10039.
10. Carlin T. J., Wise M. B., Freiser B. S.: *Inorg. Chem.* **1981**, *20*, 2743.
11. Gord J. R., Freiser B. S.: *Anal. Chim. Acta* **1989**, *225*, 11.
12. MacMahon T. J., Jackson T. C., Freiser B. S.: *J. Am. Chem. Soc.* **1989**, *111*, 421.
13. Dance I., Fisher K., Willett G.: *Angew. Chem.* **1995**, *107*, 215.
14. Dance I. G., Fisher K. J., Willett G. D.: *Inorg. Chem.* **1996**, *35*, 4177.
15. Schröder D., Kretzschmar I., Schwarz H., Rue C., Armentrout P. B.: *Inorg. Chem.* **1999**, *38*, 3474.
16. Drowart J., Pattoret A., Smoes S.: *Proc. Br. Ceram. Soc.* **1967**, *8*, 67.
17. DeVore T. C., Franzen H. F.: *High Temp. Sci.* **1975**, *7*, 220.
18. Barrow R. F., Cousins C.: *Adv. High Temp. Chem.* **1971**, *4*, 161.
19. Jackson T. C., Carlin T. J., Freiser B. S.: *Int. J. Mass Spectrom. Ion Processes* **1986**, *72*, 169.

20. Bauschlicher C. W., Jr., Maitre P.: *Theor. Chim. Acta* **1995**, *90*, 189.
21. Capron L., Feng W. Y., Lifshitz C., Tjelta B. L., Armentrout P. B.: *J. Phys. Chem.* **1996**, *100*, 16571.
22. Harvey J. N., Heinemann C., Fiedler A., Schröder D., Schwarz H.: *Chem. Eur. J.* **1996**, *2*, 1230.
23. Glukhovtsev M. N., Bach R. D., Nagel C. J.: *J. Phys. Chem. A* **1997**, *101*, 316.
24. Hübner O., Termath V., Berning A., Sauer J.: *Chem. Phys. Lett.* **1998**, *294*, 37.
25. Bärsch S., Kretzschmar I., Schröder D., Schwarz H., Armentrout P. B.: *J. Phys. Chem. A* **1999**, *103*, 5925.
26. Bärsch S., Schröder D., Schwarz H., Armentrout P. B.: *J. Phys. Chem. A* **2001**, *105*, 2005.
27. Hübner O., Sauer J.: *Phys. Chem. Chem. Phys.* **2002**, *4*, 5234.
28. Hübner O., Sauer J.: *J. Chem. Phys.* **2002**, *116*, 617.
29. Heisenberg W.: *Z. Phys.* **1928**, *49*, 619.
30. Dirac P. A. M.: *Proc. R. Soc. London, Ser. A* **1929**, *123*, 714.
31. Nesbet R. K.: *Ann. Phys.* **1958**, *4*, 87.
32. Fink K., Fink R., Staemmler V.: *Inorg. Chem.* **1994**, *33*, 6219.
33. Wang C., Fink K., Staemmler V.: *Chem. Phys.* **1995**, *192*, 25.
34. Mödl M., Dolg M., Fulde P., Stoll H.: *J. Chem. Phys.* **1997**, *106*, 1836.
35. Mödl M., Povill A., Rubio J., Illas F.: *J. Phys. Chem. A* **1997**, *101*, 1526.
36. Sugar J., Corliss C.: *J. Phys. Chem. Ref. Data* **1985**, *14, Suppl. 2*, 1.
37. Werner H.-J., Knowles P. J.: *MOLPRO, A Package of ab initio Programs* (with contributions from J. Almlöf, R. D. Amos, M. J. O. Deegan, S. T. Elbert, C. Hampel, W. Meyer, K. Peterson, R. Pitzer, A. J. Stone, P. R. Taylor, R. Lindh, M. E. Mura and T. Thorsteinsson).
38. Knowles P. J., Werner H.-J.: *Chem. Phys. Lett.* **1985**, *115*, 259.
39. Werner H.-J., Knowles P. J.: *J. Chem. Phys.* **1985**, *82*, 5053.
40. Knowles P. J., Werner H.-J.: *Chem. Phys. Lett.* **1988**, *145*, 514.
41. Werner H.-J., Knowles P. J.: *J. Chem. Phys.* **1988**, *89*, 5803.
42. Werner H.-J., Knowles P. J.: *Theor. Chim. Acta* **1990**, *78*, 175.
43. Szalay P. G., Bartlett R. P.: *Chem. Phys. Lett.* **1993**, *214*, 481.
44. Pierloot K., Dumez B., Widmark P.-O., Roos B. O.: *Theor. Chim. Acta* **1995**, *90*, 87.
45. Becke A. D.: *J. Chem. Phys.* **1993**, *98*, 5648.
46. Stephens P. J., Devlin F. J., Chabalowski C. F., Frisch M. J.: *J. Phys. Chem.* **1994**, *98*, 11623.
47. Schäfer A., Huber C., Ahlrichs R.: *J. Chem. Phys.* **1994**, *100*, 5829.
48. Wachters A. J. H.: *J. Chem. Phys.* **1970**, *52*, 1033.
49. Ahlrichs R., Bär M., Häser M., Horn H., Kölmel C.: *Chem. Phys. Lett.* **1989**, *162*, 165.
50. Treutler O., Ahlrichs R.: *J. Chem. Phys.* **1995**, *102*, 346.
51. Ricca A., Bauschlicher C. W., Jr.: *Chem. Phys. Lett.* **1995**, *245*, 150.
52. Hertwig R. H., Koch W.: *Chem. Phys. Lett.* **1997**, *268*, 345.